

Final Report to the
Thirty Meter Telescope Project

Infrared Multi-Object Spectrograph (IRMOS)
Multi-Object Adaptive Optics (MOAO) System Feasibility Study

Donald Gavel and Brian Bauman
UCO/Lick Observatory
UC Santa Cruz

September, 2006

Table of Contents

1.	Introduction to the MOAO concept	4
2.	Science Requirements and Nominal IRMOS Configuration	5
3.	MOAO Error Budget	6
3.1.	Term Definitions	6
3.2.	IRMOS/MOAO Error Budget.....	9
4.	Tomography configuration	10
5.	Stroke budgets and woofer-tweeter options.....	12
6.	Status of MEMS deformable mirrors development	14
6.1.	MEMS DM Advantages	15
6.2.	MEMS Disadvantages and Risks.....	16
6.3.	Results of Laboratory Testing of 1K Actuator Devices.....	17
7.	Open Loop Control	21
7.1.	Wavefront sensing	22
7.2.	Wavefront control	23
8.	LGS Wavefront Sensor Design.....	24
9.	MOAO Relay Design.....	26
9.1.	Consequence of no pupil relay.....	26
9.2.	Relay design.....	26
10.	IRMOS Staging Options	31
11.	References.....	32

Table of Figures

Figure 1. Multi Object Adaptive Optics (MOAO) system concept for a wide-field multi-channel IFU spectrograph.....	5
Figure 2. Left: picture of the streak of sodium return from the sodium guide star projected from the 3 meter Shane telescope, as seen from the 1 meter Nickel telescope, about 600 m to the west. Right: drift-scan image; time is resolved in the direction orthogonal to the streak.....	8
Figure 3. Typical plot of sodium centroid of height fluctuation (left) and power spectrum (right).....	9
Figure 4. An 8 guidestar constellation (stars) on a 5 arcminute diameter field. The constellation outer radius is 120 arcseconds. Ensquared energy curves are shown for science objects (squares) at 0, 75, and 150 arcsecond radius from the center of the field.	11
Figure 5. 8 guidestar constellation with a 150 arcsecond constellation radius. Note that ensquared energy curves are not as good as the 120 arcsecond case, particularly at the edge of the field.	11
Figure 6. a) 1000 actuator Boston Micromachines MEMS deformable mirror. This is a 32x32 actuator array at 360 microns pitch. b) MEMS mirror plugged into its electrical connector board with cabling shown. The green disk is the 532 nm PSDI interferometer beam.	16
Figure 7. The MEMS device test set up in the phase-shifting diffraction interferometer (PSDI) on the LAO Extreme Adaptive Optics Testbed.	17
Figure 8. Results of flattening the MEMS mirror. Left: unpowered surface. Center: Flattened surface. Right: Flattened surface with the data spatially low-pass filtered with filter cutoff at the Nyquist frequency. Note the change in scale.....	18
Figure 9. Improvements to actuator yield over the course of the 1K development project. Displayed are interferometer measured surface maps from two MEMS devices. Dark areas indicate non-responding or partly responding actuators. The white dots are fiducials added by the analysis software to indicate actuator locations.	20
Figure 10. Examples of elongated LGS Hartmann spots and the pixel geometry for the Beletic/Nelson CCD sensor design.....	22
Figure 11. Hartmann tilt measurement error of an elongated LGS spot due to pixelization nonlinearity. See text for full explanation. The graph is for tilts in the direction across the elongation. Tilt errors along the elongation direction are essentially zero on this scale. The probability distribution of open loop tilts is overplotted with a dotted line. Rms tilt errors and extrapolated rms wavefront errors are summarized in the table.	23
Figure 12. IRMOS with LGS wavefront sensors conjugate to 90 km (left) and 180 km (right).	25
Figure 13. Details of the wavefront sensors.	25
Figure 14: Two mirror general design for MOAO. Light from the telescope enters at left; the spectrograph would be at right.	27
Figure 15: Zoomed-in view of general MOAO design.....	27
Figure 16. Perspective drawing of AO relay optics, showing envelope calculations.	29
Figure 17: Envelope of MOAO buttons: height and width in arcseconds, length in mm.	30

Table of Tables

Table 1. SRD requirements for IRMOS/MOAO.....	6
Table 2. Nominal design IRMOS/MOAO parameters	6
Table 3. IRMOS/MOAO error budget.....	10
Table 4. Summary of LGS constellation performance for a variety of constellation configurations and radii. 50 mas ensquared energy percentages at $\lambda = 1$ micron science wavelength are shown for science objects at 0, 75, and 150 arcseconds radius from the center of the constellation field. The best performing constellation is highlighted.	12
Table 5. Table of MEMS flattening test results.....	18
Table 6. Results of MEMS stability and repeatability tests.....	19
Table 7. MEMS device specifications for the consortium.....	21
Table 8. Envelope calculations for IRMOS AO relay optics.....	29

1. Introduction to the MOAO concept

Astronomical adaptive optics systems have been traditionally targeted toward high resolution narrow field imaging and spectroscopy applications. This field is limited by the *isoplanatic* angle, the angle over which a single wavefront phase correction for the atmospheric aberrations is coherent at the science wavelength, and this angle is usually much smaller than the telescope's designed field of view. Telescope time however is expensive, and a means of multiplexing the science of AO observations is of interest. One way of doing this is *Multiple Object Adaptive Optics* (MOAO) where separate wavefront corrections are applied for each of several objects in the field, and the corrected images are then sent to separate imagers and/or spectrographs.

The Thirty Meter Telescope (TMT) has begun a feasibility study for the Infrared Multiple Object Spectrograph (IRMOS) instrument which will use the MOAO concept to produce high resolution images of up to 20 objects on a 5 arcminute diameter field. Separate integral field units (IFUs) will slice up these fields to produce spectral data cubes of each object. Each subfield being a 40x40 grid of 50 milliarcsecond spatial elements and the spectrograph operating at up to $R=4000$. The TMT science requirements for the spectrograph and AO system are summarized in 2.

A diagram of the generic MOAO architectural concept is shown in Figure 1. To sense the wavefront needed for AO correction a number of laser guide stars and natural tip/tilt stars are used as beacons to probe the volumetric distribution of the atmospheric index of refraction. The process is analogous to that used in medical tomography, where ray sources and detectors outside of the body are used to image volumes within it. Once the volume of index deltas is determined, the control computer performs line integrals through it from science objects to telescope aperture, the result being the proper wavefront correction for those objects. Each spectrograph arm has, in front of it and at a pupil, a deformable mirror for placing the wavefront corrections. Then the light is focused at an f-number appropriate for an IFU field slicer and the rest of the spectrograph.

MOAO has a number of advantages over other means of achieving wide field adaptive optics correction. One important advantage is the elimination of anisoplanatic error. In single deformable mirror AO systems, anisoplanatic error arises since the wavefront correction is good at only one point in the field, the direction of the guide star. In multiple conjugate AO (MCAO) systems, there is a generalized isoplanatic error due to approximating the atmospheric volume as a series of discrete layers.¹ In MOAO, each science object has its own deformable mirror with a correction determined by a line integral in that direction though the tomographically measured volume of atmosphere. A second advantage is the simplicity of the optics in the adaptive optics relay, since each relay is required only to pass a narrow field, the wide-field aberrations that occur in MCAO designs is not an issue. This leads to a third advantage, that since the field of

view for each MOAO deformable mirror is small, the Lagrange invariant* is small and a small aperture deformable mirror can be used. The small deformable mirrors we have in mind are micro-electro-mechanical systems (MEMS) with apertures of 25-40 mm. MEMS have a tremendous cost scaling advantage over traditional large aperture deformable mirror technology. The small size of the DM also drives down the overall size of the AO system, making the individual spectrograph arms compact and able to be placed at high density in the telescope's focal plane.

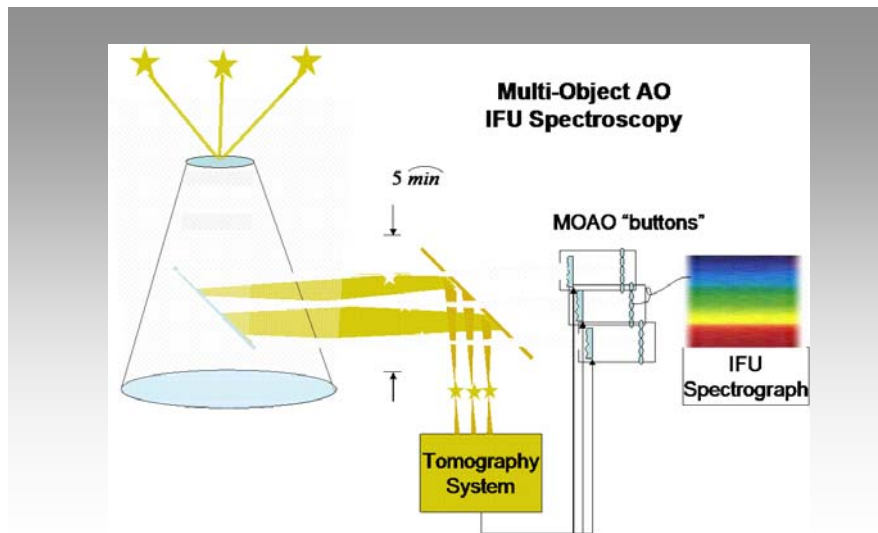


Figure 1. Multi Object Adaptive Optics (MOAO) system concept for a wide-field multi-channel IFU spectrograph.

The MOAO concept is not without disadvantages and technical challenges. The control is open-loop, since the wavefront measurement is done with light that has not reflected off of the deformable mirrors. This requires extraordinarily high linearity and accuracy of the wavefront sensors over a high dynamic range (up to 20 microns of phase measured to an accuracy of about 10 nanometers). It also requires that the deformable mirrors go to where they are commanded to go, without benefit of optical feedback from the guide stars. Both of these issues have tenable solutions which we will outline in this report.

2. Science Requirements and Nominal IRMOS Configuration

The science requirements for IRMOS and MOAO are published in the TMT Science Requirements Document (SRD).² Table 1, below, summarizes these requirements.

* The Lagrange invariant states that as the beam diameter at a pupil becomes smaller in proportion to the entrance aperture field angles are magnified proportionally.

Table 1. SRD requirements for IRMOS/MOAO

Wavelength range	0.6 to 2.5 microns
Field of View	1-5 arcsec AO corrected channel
Field of Regard	20 square-arcmin (up to 20 channels in this field)
Image/Wavefront quality	50% of the flux from a point source at $\lambda = 1\mu$ into a 0.05 arcsec square
Sky coverage	>90% at the Galactic poles
Background	<15% over natural sky+telescope

The AO system is actually not required to produce a diffraction-limited image, but is required to convey at least 50% of the light from a point source into a 50 milliarcsecond (mas) square. For the most part, it is necessary to achieve reasonably high high-order Strehl in order to accomplish this (for comparison, the seeing disk is about 500 mas while the diffraction-limit, at 1 micron wavelength, is about 7 mas) so that the instantaneous PSF will have a single bright central core. On the other hand, the demands on tip/tilt correction are relaxed considerably, allowing so to speak up to 25 mas rms tip/tilt error. This will enable IRMOS/MOAO to use visible light natural tip/tilt stars, instead of AO corrected IR tip/tilt stars, and also enable the specifications to be met over a large fraction of the sky.

Nominal parameters for the MOAO system that will meet SRD requirements are given in Table 2.

Table 2. Nominal design IRMOS/MOAO parameters

Number of laser guide stars	8 in a 5+3 configuration (two circles, one with 5 guidestars at 2.5 arcminute radius and one with 3 guidestars at 1.25 arcminute radius)
Number of natural tip/tilt guide stars	4
Tip/tilt sensing wavelength	J band
DM degrees of freedom	Baseline SRD: 10,000 (100x100) Descope option 1: 4,096 (64x64) Descope option 2 (H+K): 1,024 (32x32)

3. MOAO Error Budget

3.1. Term Definitions

The multiple object adaptive optics system has the following fundamental error budget terms:

Tomography error – the error in measuring the volume of atmospheric turbulence given a constellation of guide stars. The error is expressed as a wavefront error that depends on field angle after integrating through the volume at that field angle. For this error it is assumed that guide stars are infinitely bright and that the tomographic reconstruction has infinite resolution in all three dimensions (pupil u,v plane and altitude, z). Limiting case scaling laws for tomography error in the infinite aperture and plane wave case are derived in the paper by Tokovinin and Viard³ and further studied for the case of finite apertures and cone beams in the paper by Gavel⁴. A reasonable scaling law for tomographic wavefront residual error is:

$$\sigma^2 = \Theta^{5/3} r_0^{-5/3} \delta_K^{5/3} \varepsilon(\theta)$$

where σ is the standard deviation of the wavefront, in radians, Θ is the average separation of guidestars in the constellation, r_0 is the Fried parameter and δ_K is the *equivalent layer thickness*, which depends on the C_n^2 profile. Monte-carlo simulations of multiple LGS tomography can determine reasonable values for this number. For the nominal, Cerro-Pachon C_n^2 profile used in this study, the equivalent layer thickness is about 900 meters. The $\varepsilon(\theta)$ factor is a field-dependent term that is nominally one at the field location of any guide star and slightly larger than one in between guide stars.

3.1.1. Fitting error

Fitting error depends on the number of degrees of freedom in the deformable mirror. It is given by

$$\sigma^2 = \mu(d/r_0)^{5/3}$$

where d is the subaperture diameter and μ is a parameter that depends on the type of deformable mirror. For continuous face sheets, μ is approximately 0.3.

3.1.2. Bandwidth error

$$\sigma^2 = (f_g/f_c)^{5/3}$$

where f_g is the Greenwood frequency, which is proportional to the wind velocity of the turbulent layers, and f_c is the closed loop bandwidth, which is usually about a factor of 10 lower than the control loop sample rate. This formula is reasonably accurate even for open loop systems – f_c is simply interpreted as a control cutoff frequency, which, even in open loop is about 1/10 the sample rate.

3.1.3. Measurement signal-to-noise error

Measurement error, in radians of phase at the science wavelength λ , is approximately

$$\sigma = \eta(d/\pi\lambda)(\sigma_{spot}/SNR)$$

where σ_{spot} is the apparent size of the Hartmann spot on the sky, SNR is the signal-to-noise in the wavefront sensor slope measurement, λ is the science wavelength, d is the subaperture diameter, and η is the noise propagator, which is a factor that is on the order of 1.5 for the 10,000 degree of freedom MOAO system.

3.1.4. Tip/Tilt error

For a study of the tip/tilt error, the reader is referred to the report by Richard Clare, “Sky Coverage Results for IRMOS.”⁵

3.1.5. Focus error

The focus term of the laser guide star measured wavefront is sensitive to variations in height of the Sodium layer. The depth of field of the TMT at 90 km is about 9 meters, therefore Sodium layer variations on the order of 9 meters, about 1/1000 of the layer’s nominal thickness, would put an unacceptable amount of wavefront error on the AO correction. To avoid this error, a separate measure of focus using a natural guide star is required. The temporal power spectrum of the variations will determine how often this measurement needs to be made. Lidar measurements⁶ show the Sodium height fluctuates by kilometers on 5 minute time scales. The spectrum falls off with a roughly -1.6 power law in height variance (m^2/Hz) in the range from $10^{-4.5}$ to $10^{-2.5}$ Hz (shortest time scales = 5 minutes). Extrapolating this spectrum, by decades, to the 1000 Hz time scale would indicate that the LGS focus component is not at all useful for wavefront reconstruction, and focus sensing of a natural star in real time is required.

Recent measurements performed at the Lick observatory have provided Sodium layer height fluctuation data down to time scales of one second. On 19 November, 2005, we viewed the Laser guide star from another telescope, about 600 meters west of the one projecting the laser, and collected focal plane images of the sodium layer fluorescence. The angle was such that we could resolve the layer into about 100 bins, or about 100 meters. Then, by drift-scanning in a direction perpendicular to the laser track, the CCD could resolve Sodium layer variations on a one second time scale.

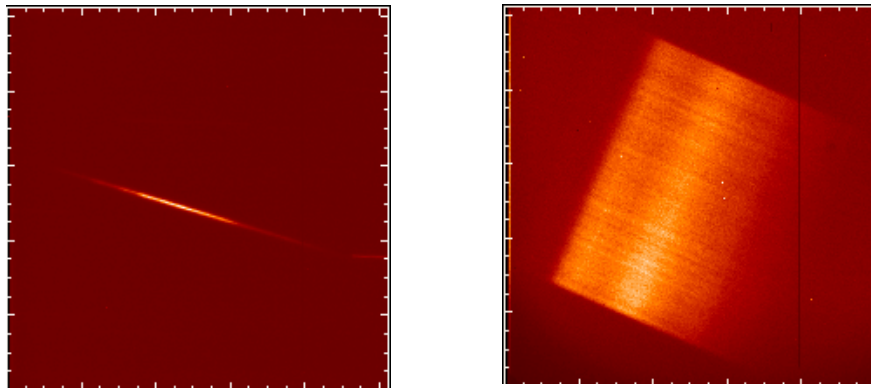


Figure 2. Left: picture of the streak of sodium return from the sodium guide star projected from the 3 meter Shane telescope, as seen from the 1 meter Nickel telescope, about 600 m to the west. Right: drift-scan image; time is resolved in the direction orthogonal to the streak.

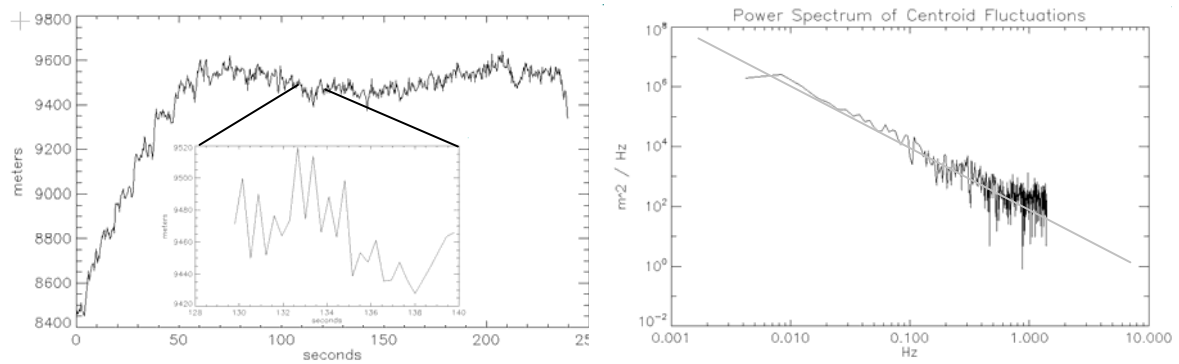


Figure 3. Typical plot of sodium centroid of height fluctuation (left) and power spectrum (right)

The data are consistent with a -2 power law in height variance (m^2/Hz) in the 0.01 to 1.0 Hz range. 20 to 40 meter excursions occur at one second time scales, so, by extrapolation we might conclude that the, say, 1 meter excursions would be occurring on a 0.01 second time scale, and focus updates should occur at about this rate. We should caution that this data set consists of one night's observations and that further data gathering will be necessary before conclusions can be made. Additional observations of the laser from the Nickel telescope will take place during LGS runs in 2006.

3.2. IRMOS/MOAO Error Budget

The preliminary IRMOS/MOAO error budget is summarized in Table 3. This error budget is preliminary and does not include some unknown errors such as focus error due to sodium layer height variability discussed above, and the nonlinearities in wavefront sensing which are discussed in a later section.

Table 3. IRMOS/MOAO error budget

Higher Order WF (nm)		
Fitting	77.66	100 actuators across DM
Aniso	0.00	(on-axis)
Tomography	159.97	
Meas	40.00	180 photocounts/subap/fram
Bandwidth	44.66	1 kHz wavefront sample rate
Total High Order	187.66	nm
Tip/Tilt (mas)		
Tilt Aniso	14	90% sky coverage
Meas	<1	J = 21
Bandwidth	<1	t = 0.8 ms
Total Tip/Tilt	14	mas
Sky Coverage		90% at NGP

Telescope diameter	D	30	m
Wavelength of parameter definitions	λ_0	500	nm
Coherence cell size	r_0	0.15	m
Greenwood frequency	f_g	50	Hz
Controller frequency	f_c	100	Hz
Outer scale	L_0	>30	m
Vertical Turbulence Profile	C_n^2	Cerro Pachon 7-layer	
Isoplanatic angle	θ_0	2.45	arcsec
LGS constellation radius	Ξ	120	arcsec
Number of guidestars	N_{gs}	8	
Science field	θ	10	arcsec
Number of DMs	N_{DM}	2	
Actuator spacing, DM 0	d	0.29	m

4. Tomography configuration

Given the rapid rise of tomography error with guidestar separation angle, it is a challenge to find a constellation that will achieve reasonable measurement over the 5 arcminute MOAO field using a reasonably small number of guide stars. We have studied a number of cases where we varied the constellation configuration, size, and number of guide stars^{7,8}. Some of the constellations are shown in Figures Figure 4 and Figure 5 and performance results are summarized in Table 1.

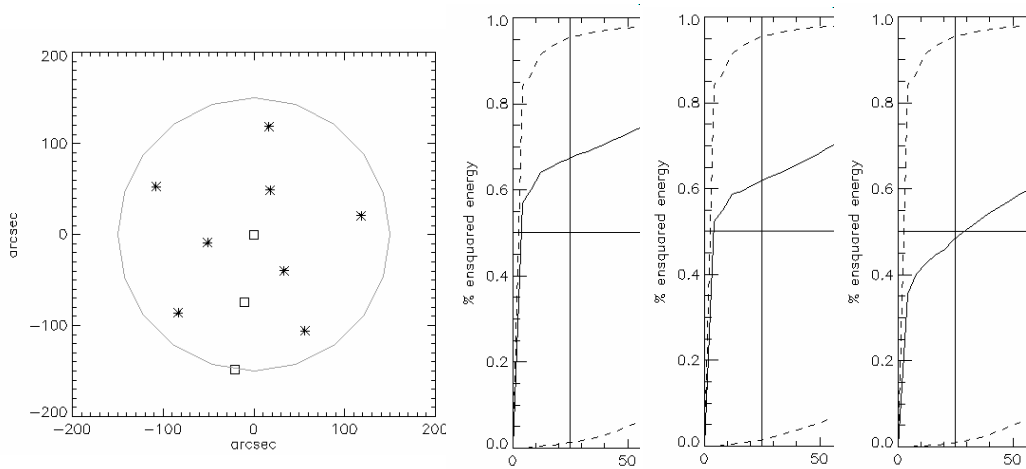


Figure 4. An 8 guidestar constellation (stars) on a 5 arcminute diameter field. The constellation outer radius is 120 arcseconds. Ensquared energy curves are shown for science objects (squares) at 0, 75, and 150 arcsecond radius from the center of the field.

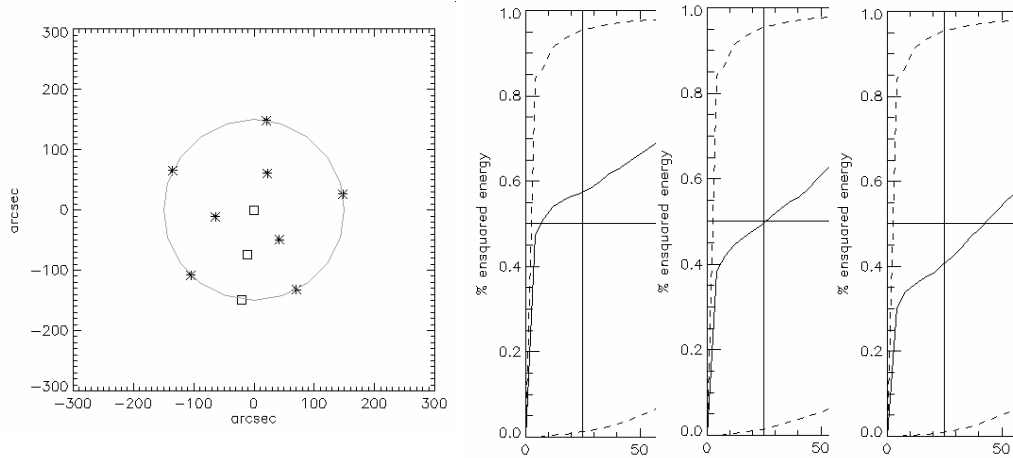


Figure 5. 8 guidestar constellation with a 150 arcsecond constellation radius. Note that ensquared energy curves are not as good as the 120 arcsecond case, particularly at the edge of the field.

Table 4. Summary of LGS constellation performance for a variety of constellation configurations and radii. 50 mas ensquared energy percentages at $\lambda = 1$ micron science wavelength are shown for science objects at 0, 75, and 150 arcseconds radius from the center of the constellation field. The best performing constellation is highlighted.

In 50 mas square at $\lambda=1$ micron

Constellation	Outer diameter, arcsec	%ee 0	%ee 75	%ee 150
5+3	150	0.6	0.5	0.4
5+3	200	0.42	0.3	0.3
5+3	120	0.7	0.62	0.5
4+3	120	0.65	0.5	0.4
5+1	120	0.48	0.4	0.3
5+2	120	0.65	0.5	0.35
6+2	120	0.6	0.6	0.45

5. Stroke budgets and woofer-tweeter options

On a 30 meter aperture telescope, an atmosphere under modest seeing conditions ($r_0 = 16$ cm) will demand a DM surface stroke range of about 10 microns. Present technology MEMS DMs do not have this entire range available, thus a second DM, denoted as a “woofer,” must be used to handle some of the stroke range.

These are the basic options for a woofer:

1. Adaptive secondary.

The goal of the telescope design is to not preclude eventual mounting of an adaptive secondary mirror (AM2). This mirror would have up to 3000 degrees of freedom and would relegate the residual high order and field dependent AO correction to the MEMS mirrors in the MOAO system.

Advantages of this approach are:

- a) Each MOAO channel would only need one DM, and a minimum of associated relay optics, for each spectrograph channel, which maximizes throughput, minimizes emissivity, and reduces overall system complexity.
- b) Wavefront sensors would see a partially corrected beam, which lowers the dynamic range required on open-loop wavefront sensing. Knowledge of the exact AM2 wavefront correction is necessary, but prior adaptive secondary mirror designs have included position sensors on the actuators to provide this information.
- c) The common woofer would enable MEMS devices with limited stroke to perform the residual correction. This residual could be handled by present day available 2 micron stroke MEMS devices.

A disadvantage of this approach is that AM2 is not slated for first light, making AO systems that are dependent on it useless until AM2 is commissioned.

2. Common woofer option A (Offner relay).

The common woofer is a single low-order DM that provides partial correction over the 5 arcminute diameter IRMOS field of regard. A concept using an Offner relay has been presented by one of the IRMOS teams (Caltech).

The *advantages* of this approach are the same as for AM2 but without having to wait for AM2 to be commissioned.

Disadvantages of this approach are

- a) It introduces from 3 to 5 additional optical surfaces in the science path, which negatively impacts emissivity and throughput.
- b) It requires building a relatively expensive conventional (piezo actuator) DM for a purpose that would be made obsolete when AM2 comes on line
- c) It requires large optical elements, ~300mm Offner relay parabolas, plus a 9 meter optical path, which makes servicing and stability an issue.
- d) If the laser guidestar wavefront sensing is relegated to after this relay, the LGS wavefronts will suffer from a severe form of non-common path aberration introduced by the relay. This is due to the fact that the relay is designed to image optics at infinity rather than the LGS focus (up to 2.6 meters behind telescope focus). This aberration is large and would have to be calibrated out rather precisely in order to perform adequate AO correction.

3. Common woofer option B (NFIRAOS).

This approach uses the Narrow Field AO system's (NFIRAOS) output field as the input feed to IRMOS. The DMs within NFIRAOS, already a woofer-tweeter pair, could then function as the common woofer for IRMOS. Potentially this might allow a "no MOAO" option since the DM pair in NFIRAOS produces a relatively wide MCAO corrected field that could feed the IRMOS channels directly,.

The main *advantages* of option B are

- a) Independence from AM2 without having to build another large relay.
- b) Using the NFIRAOS wavefront sensors instead of building a separate set for IRMOS/MOAO would save on cost.
- c) The no MOAO option could eliminate the need for DMs and AO relays in each IRMOS channel. It is yet to be determined whether the SRD specifications can be met in this configuration. It may be necessary to preserve the option to upgrade to DMs in each channel, which would then mean keeping the AO relays and blank positions for DMs (populated by flat mirrors) in each channel anyway.

Disadvantages of option B are

- a) The conceptual design for NFIRAOS has only a 2 arcminute output field of regard, significantly less than the SRD requirement of 5 arcminutes.
- b) NFIRAOS introduces at least 4 additional surfaces in the path of the science light, which negatively impacts emissivity and throughput.

4. Woofer tweeter pair in each arm.

In this configuration, each MOAO channel has one woofer DM and one MEMS DM (the “tweeter”). The woofer DM needs to be small in physical size to keep the overall size of IRMOS manageable. There are a number of commercial options for small low-order DMs, falling into three basic categories: piezo-bimorph, silicon membrane MEMS, or magnetic actuator MEMS. Since each MOAO channel has a small field of view, it is not necessary to have a separate pupil relay for the woofer – it can live in the same optical space as the MEMS mirror.

Advantages are

- a) This option makes IRMOS/MOAO independent of AM2.
- b) It precludes the need for using a large common woofer relay (either Offner or IRMOS), saving the extra reflections and corresponding negative impact on emissivity and throughput, and saving the extra cost of the Offner relay.
- c) It allows the wide field of regard specified in the SRD.
- d) The LGS wavefront sensors have very little non-common path aberrations introduced by a relay.

Disadvantages are:

- a) Extra cost of woofer DMs for each channel.
- b) The individual small woofer DMs will each have fewer degrees of freedom than would be on a large common woofer. This will increase the stroke needed on the MEMS tweeter beyond the 2 micron stroke available on current technology devices. The MEMS consortium is working to develop a 4 micron stroke device which will mitigate this.
- c) If the woofer DM used is a piezo-bimorph, its “go-to” shape will need to be sensed with an interferometer for precise open-loop wavefront control. A small interferometer system has been designed to handle this (LAO’s “mini-QPI”), but this adds complexity and cost.

6. Status of MEMS deformable mirrors development

The Laboratory for Adaptive Optics, in collaboration with the Center for Adaptive Optics, Gemini Observatory, and the TMT project, is pursuing the development of micro-electro-mechanical system (MEMS) technology suited for adaptive optics for large aperture telescopes. Currently, the most promising design is from the Boston Micromachines Corporation (BMC), which has shown good progress in making highly reliable, high yield, and nominally flat deformable mirrors with high actuator count. This device consists of discrete electrostatically controlled actuators each with a stiff post attached to a continuous top plate in order to exert force and therefore deflect the plate. The plate is coated with either aluminum or gold in order to form a reflective surface.

6.1. MEMS DM Advantages

MEMS technology provides a number of advantages over conventional deformable mirror approaches:

- Small size – microfabrication on silicon wafers allow very small inter-actuator separation, on the order of 400 microns on the devices we are testing.
- High actuator count at reasonable cost – The marginal cost of scaling to high actuator counts is considerably lower than that for large DMs. For the BMC devices, this number today appears to be around \$200-300 per actuator as compared to about \$1500 per actuator on a piezoelectric deformable mirror. These numbers include the cost of drive electronics. The two numbers we have from BMC are ~\$30K for a 144 actuator device which is available off the shelf, and ~\$1M for delivery of a 4,000 actuator device they are now developing for us as part of the Gemini Planet Imager project. This later project includes the non-recurring expense of developing the chip and package, so we expect that its cost of reproduction will go down considerably. Given some rough order of magnitude estimates from Paul Bierden, president of BMC, for the cost of fabricating wafers, packaging, bonding, and the known cost of drive electronics, we can expect costs to drop to about \$40 per actuator, or about \$400K for a 10,000 actuator device.
- “Go-to” repeatability – One major advantage of an electrostatic actuation over piezoelectric actuation is the absence of hysteretic effects in the displacement to voltage response curves. This implies that the devices could be driven open loop to given surface deflections. Open-loop tests of stability and repeatability are presented in Section 6.3.2 below.

The low cost and small size of MEMS DMs opens up the possibility of “ubiquitous MEMS,” i.e. devices sprinkled throughout the system to elegantly solve tough optical problems.

- MEMS DM in each wavefront sensor: This creates a mini closed-loop AO system in which the wavefront detector is kept near null, where its linearity properties are best. The predictable voltage response of the MEMS allows it to be used as the probe of the grosser portion of the wavefront shape, which would be added to the wavefront sensor’s residuals to complete the wavefront measurement.
- MEMS in the tip/tilt sensors: If there are enough degrees of freedom to form diffraction limited cores at the sensing wavelength, fainter guide stars can be used to sense tip/tilt to a given accuracy because centroid error is proportional to the spot size and inversely proportional to square root of brightness. The ability to use fainter guide stars would give us higher sky coverage. Although our baseline for IRMOS does not need to take this approach, since the encircled energy requirements are relaxed enough to allow tip/tilt sensing using unsharpened stars in the J band, this concept could be used to advantage in more stressing AO design concepts, such as NFIRAOS diffraction limited imaging or in an IRMOS

high-Strehl “superbutton,” where a long exposure diffraction limited PSF is desired along with good sky coverage.

- MEMS in the laser projector: Uplink correction, i.e. correction of the laser wavefronts for the distortions they will see along the upward path through the atmosphere, will produce smaller illuminated spots in the Sodium layer. There would need to be one DM per beam, since each goes through a different atmospheric path, and the small size of the MEMS lends itself well to placement in a pupil conjugate in the laser paths ahead of the launch telescope.

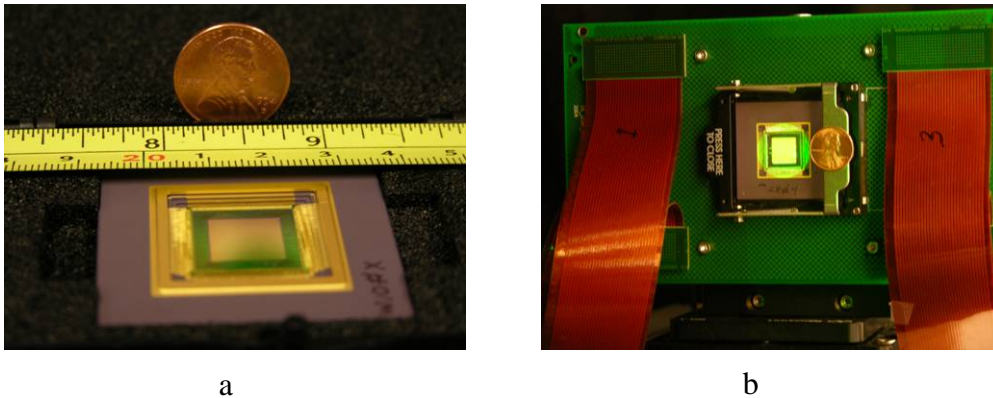


Figure 6. a) 1000 actuator Boston Micromachines MEMS deformable mirror. This is a 32x32 actuator array at 360 microns pitch. b) MEMS mirror plugged into its electrical connector board with cabling shown. The green disk is the 532 nm PSDI interferometer beam.

6.2. MEMS Disadvantages and Risks

MEMS technology is fairly new, and as such, presents a development risk.

- Limited stroke – present technology for the electrostatic actuator is at about 4 microns surface deflection, compared to the approximately 10 microns needed for the 30 meter aperture of TMT. To work around this in a design, a second low-order high stroke deformable mirror, or “woofer” mirror, must be placed in the path. Fortunately, the amplitude of the Kolmogorov atmospheric wavefront spectrum falls rapidly with spatial frequency so the majority of the stroke is concentrated at the low spatial frequencies.
- Reliability – The BMC MEMS mirrors, as well as some woofer mirrors, have been field tested where conditions are similar to those found in a dome/mountaintop environment.⁹ MEMS have also been extensively life-cycle tested in the laboratory. BMC has done billion-actuation tests of their actuator with no evidence of fatigue. However, MEMS have not yet been proven in routine astronomical telescope use and the reliability and failure rates have yet to be proven convincingly for astronomers.
- Yield – Yield relates ultimately to per device cost, and with the yield not yet known for 4000 and 10000 actuator devices we have difficulty stating the cost.

BMC has made considerable progress increasing the yield on their 1000 actuator devices under the earlier development contract with LAO. Similar results in yield will undoubtedly lead to a per unit cost factors of 10 below piezo DMs.

- Vendor sources – In today’s market, MEMS providers are generally small companies, often associated with the telecom industry, as opposed to large aerospace firms with considerable experience producing conventional technology DMs.

The fact that a new technology has never been used in astronomy before should certainly not be a deterrent to astronomers pioneering its use. As an example, the application of CCDs as astronomical detectors in the 1970’s provides a precedent where tremendous breakthroughs in science can be achieved using new technologies in new instruments.

6.3. Results of Laboratory Testing of 1K Actuator Devices

A number of 1,000-actuator MEMS devices have been delivered to the LAO for testing. These mirrors have a surface stroke of up to 2 microns with a 200V actuation applied. We tested the devices for long stability and repeatability of surface figure using a very precise point diffraction interferometer. We also flattened the surface and measured the spatial frequency distribution of the residual as well as the resulting point spread function in the far field.^{10,11}

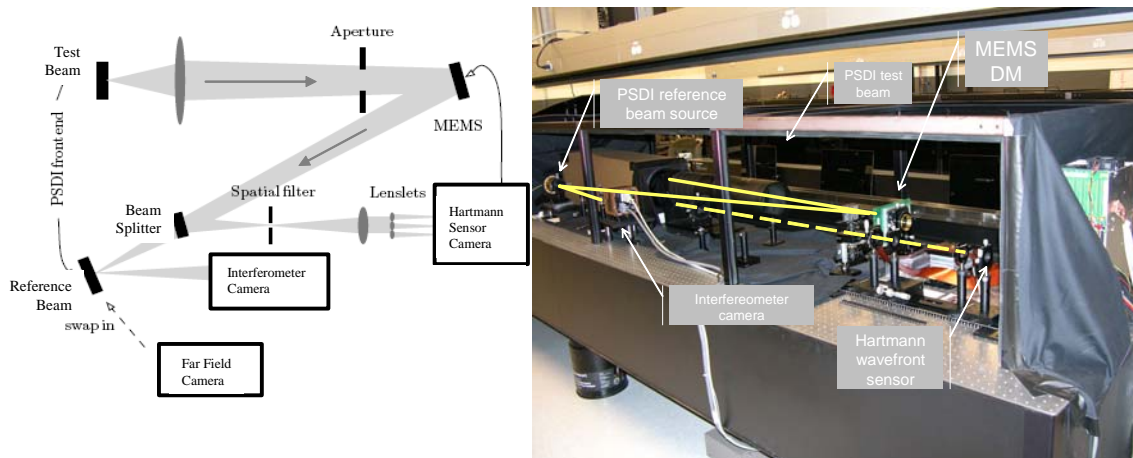


Figure 7. The MEMS device test set up in the phase-shifting diffraction interferometer (PSDI) on the LAO Extreme Adaptive Optics Testbed.

6.3.1. Mirror Flattening

Typical MEMS mirror flattening performance is shown in Figure 8. The unpowered mirror reflected wavefront has 148.1 nm phase departure from flat, mostly low-order aberration as shown. After flattening, the mirror has 12.8 nm of wavefront error, with 0.54 nm located inside the Nyquist sampling spatial bandwidth of the actuators. Thus approximately 12 nm is attributed to “orangepeel” and other micro roughness at spatial frequencies above Nyquist. This is comparable to the best piezo actuated mirrors, where

after-correction surface roughness of about 10 nm rms phase has been reported. 30 nm rms post-correction phase is typical with piezo DMs in present day astronomical AO systems.

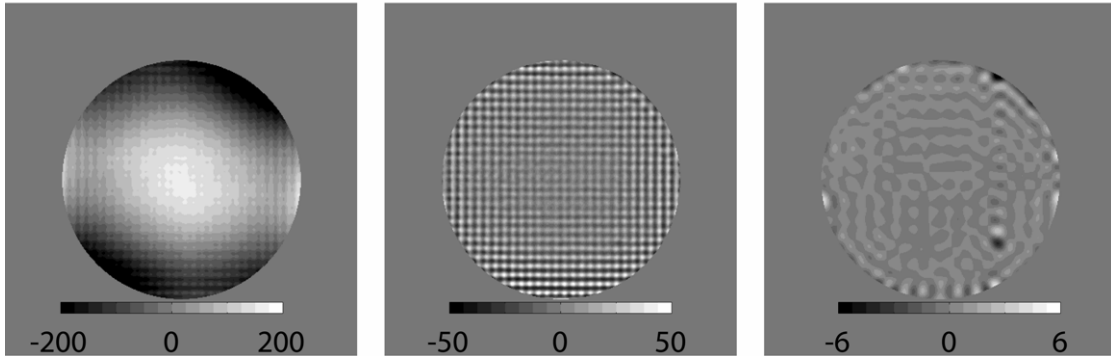


Figure 8. Results of flattening the MEMS mirror. Left: unpowered surface. Center: Flattened surface. Right: Flattened surface with the data spatially low-pass filtered with filter cutoff at the Nyquist frequency. Note the change in scale.

Table 5. Table of MEMS flattening test results

	Unpowered	Flattened
Total rms wavefront error	148.1 nm	12.8 nm
rms wavefront error in band	144.1 nm	0.54 nm

6.3.2. Stability and Go-to Repeatability

As a test of long term stability we gave the MEMS a fixed set of voltage commands and took differences of interferometer-measured wavefronts over various time scales between a minute and roughly half an hour. These were compared to similar measurements using a test flat. To test go-to repeatability, we measured the surface at a given command position, then moved the MEMS to flat, then returned to the command position. This was repeated for several cycles over a time span of roughly an hour. Anecdotally, the go-to repeatability does not appear to change even over days (additional long-term tests will be performed to confirm this). Results of these tests are summarized in Table 6.

Table 6. Results of MEMS stability and repeatability tests.

- 96% of the actuators display quadratic voltage-displacement curves.
- Go-to capability:
 - 97% of the actuators tested went to a commanded shape to under 1.0 nm phase
 - 73% of the actuators tested went to a commanded shape to under 0.4 nm phase
- MEMS Stability:
 - 0.088 nm phase over 1.33 min.
 - 0.106 nm phase over 8 minutes.
 - 0.150 nm phase in 38 minutes.

62% of actuators* were stable to under 0.1 nm phase stddev.

89% of actuators were stable to under 0.2 nm phase stddev.

96% of actuators were stable to under 0.3 nm phase stddev.

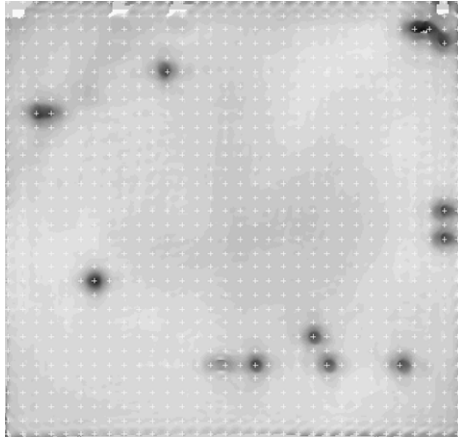
*By “actuator” we mean average surface height over one interactuator spacing sized area, centered on an actuator

- Reference flat mirror, for comparison:
 - 0.042 nm phase over 0.33 min.
 - 0.116 nm phase over 8 min.
 - 0.122 nm phase over 38 min.

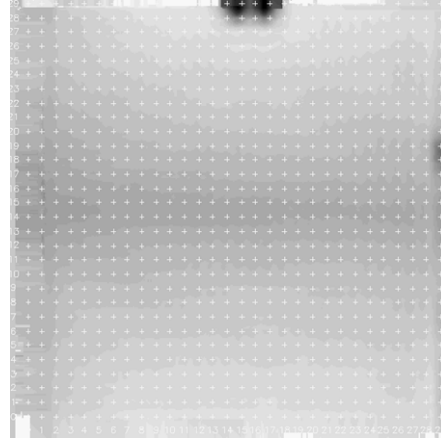
Instrumental error of the PSD Interferometer is on the order of 0.2 nm per measurement. Errors in the numbers reported above were beaten down by repeated measurements and fitting to trend lines.

6.3.3. Actuator Yield

Considerable effort by the manufacturer has gone into refining the silicon micromachining process so as to yield a higher percentage of working actuators. “Failed” actuators actually fall into a number of categories including completely stuck, floating, and shorted as pairs. As can be seen from Figure 9, our latest devices are getting a reasonably large aperture clear of actuator defects.



Early Device. Fall 2004



Device W107#X. Fall 2005

Figure 9. Improvements to actuator yield over the course of the 1K development project. Displayed are interferometer measured surface maps from two MEMS devices. Dark areas indicate non-responding or partly responding actuators. The white dots are fiducials added by the analysis software to indicate actuator locations.

6.3.4. Actuator Temporal Frequency and Step Response

Tests by Boston Micromachines show a 90% step response of 400 microseconds and a 2.8 kHz 6db frequency roll-off at for actuators on the 1K device.¹² This performance should be sufficient for IRMOS AO application. The challenge will be to preserve the response on the 4K/10K device design. The consortium specification (see below) is a 200 Hz bandwidth, which could be achieved if the manufacturer can match the 1K device curves.

An issue for IRMOS is how the device might operate in vacuum, without the benefit of air dampening. It is possible to tailor the frequency roll off of the voltage signal so as to introduce the dampening artificially. This might require special design and tuning of the drive amplifiers however.

6.3.5. MEMS Development Consortium

The Laboratory for Adaptive Optics is leading a consortium to develop a 4000 actuator continuous face sheet deformable mirror with Boston Micromachines Corporation. This development phase builds on earlier work that successfully produced a 1000 actuator DM which is now completing tests at the LAO. Specifications of the 4000 actuator device are summarized in Table 7 below. The principle product of this consortium effort is a 4096 element device for use in the Gemini Planet Imager (GPI). With TMT, CfAO, and LAO as partners however the actuator specifications are also appropriate to a TMT 10,000 actuator device. As part of the contract, BMC will do the design for the 10,000 actuator chip and package, which can be followed on by a contract for their fabrication. The development model is that once the actuator design, yield, and routing/cabling issues have been resolved for a 4K device, it is straightforward engineering to scale up to the

10K device. As mentioned earlier, it is expected that the per-unit cost of a 10,000 actuator device would be on the order of \$400K, including drive electronics.

Table 7. MEMS device specifications for the consortium

<i>TMT mirror:</i>	
Actuator spacing ¹	300-600 microns (clear aperture 20-60 mm)
Number of actuators ²	10,000 (100x100)
Stroke range	4 microns surface required, 6 microns goal
Closed loop bandwidth	>200 Hz
First resonance	>2000 Hz
Go-to accuracy open loop	<10 nm
Surface quality	<10 nm RMS
Unpowered Flatness	<70 nm RMS after tilt and sphere removed
Print-through	as small as feasible
Neighboring actuator differential stroke	>1 micron
Reflective surface	Continuous face sheet, coated with Gold
Operating temperature	As low as -30 degrees Celsius
Yield	99% of actuators working to full specification
Notes:	
1) Actuator spacing: A 60 mm clear aperture is required for the multi-conjugate adaptive optics (MCAO) system, a first-light TMT instrument where the present baseline is to use conventional DMs. 20 mm clear aperture is adequate for the multi-object adaptive optics (MOAO) system, which may become a first light instrument if MEMS are available.	
2) Number of actuators: The final goal for meeting the TMT science requirements is a 10,000 actuator DM. A device with 4,096 actuators however is considered a serious "entry level" device that might be useful on TMT AO instruments.	

The consortium MEMS contract is in three phases. Phase 1 is development of the actuator that meets our specifications. Phase 2 is design of the packaging, and Phase 3 is fabrication and packaging of the final 4096 actuator device for GPI and completion of a design for the 10,000 actuator device. The Phase 1 portion of the contract has already been let and first test devices are due out of foundry in March 2006. The entire contract through Phase 3 will be completed by the end of year 2007.

7. Open Loop Control

One of the unique features of the IRMOS concept is the necessity for open loop wavefront sensing and control. To accomplish this, both the wavefront sensor and the deformable mirror must be linear (strictly speaking, linearizable, perhaps with lookup tables) over the entire dynamic range of phase aberration expected in uncorrected seeing conditions. For IRMOS this means open loop sensing and control of up to 20 microns of optical path to an accuracy of roughly 100 nm.

7.1. Wavefront sensing

We will assume that the specialized Hartmann wavefront sensor design proposed by Jerry Nelson and Jim Beletic is used. This detector has the pixels arranged such that the radially elongated laser guide star spots are aligned along the grid of pixels. Furthermore, we assume that the laser is CW, and hence the centroid of the elongated spot on the detector must be calculated. Examples of the geometry of particular spots are shown in Figure 10. As the spot deflects from its nominal position due to atmospheric seeing, there will be a pixelization error, which will manifest itself as a nonlinearity of the read out tilt motion vs true tilt motion. Representative plots of the x (across the elongated spot) and y (along the elongated spot) tilt measurement error due to nonlinearity are shown in Figure 11. It is assumed that the initial offset bias is subtracted and that the tilt readout is normalized to a slope of one at small deflections. Curves are shown for various numbers of pixels assigned to the Hartmann subaperture. The elongation chosen for these simulations, 2.56 arcsec, is the area-weighted elongation over the 30 meter aperture for a guide star at zenith. The overplotted dotted line shows the probability distribution of open-loop wavefront tilts over a subaperture in these seeing condition ($r_0 = 16$ cm).

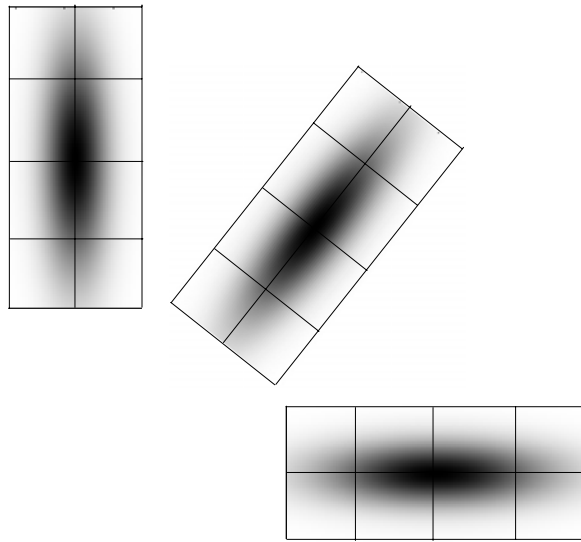


Figure 10. Examples of elongated LGS Hartmann spots and the pixel geometry for the Beletic/Nelson CCD sensor design.

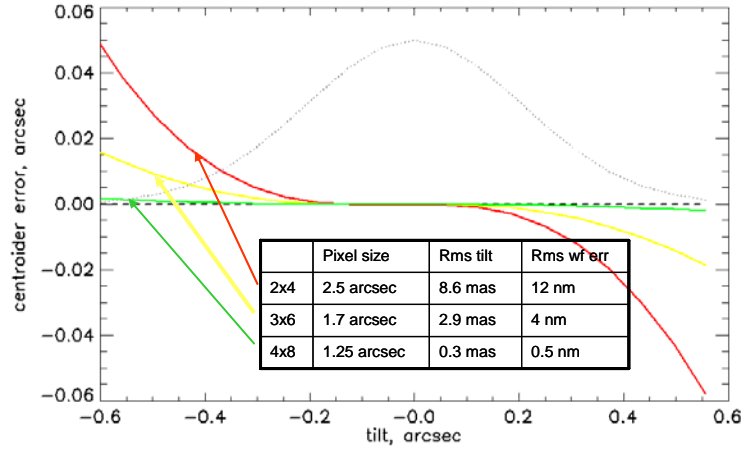


Figure 11. Hartmann tilt measurement error of an elongated LGS spot due to pixelization nonlinearity. See text for full explanation. The graph is for tilts in the direction across the elongation. Tilt errors along the elongation direction are essentially zero on this scale. The probability distribution of open loop tilts is overplotted with a dotted line. Rms tilt errors and extrapolated rms wavefront errors are summarized in the table.

The table in the graph shows rms tilt error due to the nonlinearity (averaged according to the probability distribution) and an extrapolation to the equivalent rms wavefront error over the entire aperture, assuming a noise propagator of unity in the wavefront reconstruction. This noise propagator is likely to be closer to 1.5 for a 10,000 actuator system, using Noll's formula¹⁵ for Hartmann slope to phase sensors: $noise\ propagator = 2(0.0068 + 0.0796 \ln(N_{dof}))$. Also, the open loop slopes, and hence the nonlinearity errors, will be systematically correlated, so the noise propagator concept, which assumes independent errors, does not strictly apply. Regardless, it is evident that the effect of nonlinearity in open loop wavefront sensing is a small, though not negligible, contribution to the error budget.

7.2. Wavefront control

MEMS deformable mirrors have the wonderful property that since the physics of their actuation is based solely on electrostatic attraction and the elastic deformation of silicon, the actuation is almost perfectly repeatable. However, surface deflection is certainly not linear with voltage, and the response of a given actuator depends on the position of neighboring actuators. Thus there remains the problem of determining the voltage commands (unique though they are) that will produce a given mirror surface shape. This problem can be attacked both empirically and theoretically, and this is a report of work in progress.

Empirical calibration involves measuring the voltage response curve of a given actuator and all of the interactions with neighboring actuators, under the perhaps reasonable assumption that further distant actuators are effectively "shielded" by the neighbors. Some initial work has been performed at LAO to try to determine the accuracy of assuming superposition of actuator responses. We are continuing to work on this with additional measurements of pairs of actuators.

An alternative is a theoretical modeling approach which assumes the thin plate approximation for deformations of the continuous top surface in response to forces, and uses separate models for the force vs voltage relationship of the individual actuators. Curt Vogel began this work using simplified actuator models¹⁴. We now believe we have an approach that uses the plate equation for the top surface combined with empirically measured models for the actuators. This has a distinct advantage over having to model the actuators since the actuator design in the MEMS device is very complicated in its details and therefore is not easy to model as simple electrostatic membrane deflection plates. The plate equation for the top surface is still a good approximation however. The plate equation is linear in applied forces so if we can treat the actuators as force controllers, the deformation of the surface is linear and superposable. This work is ongoing in the LAO and we are confident that the mathematical details will be worked out and a laboratory demonstration of the technique will take place by the end of this contract. We also anticipate that the real-time implementation of the solution will require on the order of number of actuators times a few iterations of a conjugate gradient algorithm. This type of algorithm is very amenable to implementation with massively parallel gate array logic, similar to real-time control implementations in the AO tomography reconstructor.

8. LGS Wavefront Sensor Design

In the IRMOS/MOAO concept, guidestar light is picked off ahead of the instrument. Figure 12 shows one concept with vertically mounted IRMOS enclosure and wavefront sensors. The vertical mounting simplifies the implementation of field rotation. The IRMOS instrument can rotate with the field, while the LGS wavefront sensor unit rotates independently with the guide star constellation, since this constellation might be fixed with respect to the pupil.

The ray trace begins at lower left, at the edge of the primary. A 45° fold mirror reflects the beam upwards towards the dichroic. The science light transmits through the dichroic to the IRMOS buttons, which are located on a drum that rotates around a vertical axis for tracking. The LGS light reflects off the dichroic, a fold mirror, and is then collimated after focus onto a mirror located at a pupil, possibly a MEMS DM. The light is then reflected downward. A subsequent relay images the pupil onto the lenslet array in a SH WFS. The small boxes are 200 mm cubes and represent the WFS CCD. The WFS's are located on another vertically-oriented rotating drum. Envelope dimensions are shown. The distance from the edge of the primary to the center of the fold mirror is 1.0 meter, and the distance from the center of the fold mirror to the science instrument is 4.0 meters (cf. 0.5m and 4.5 m dimensions above to the edges of the mirrors).

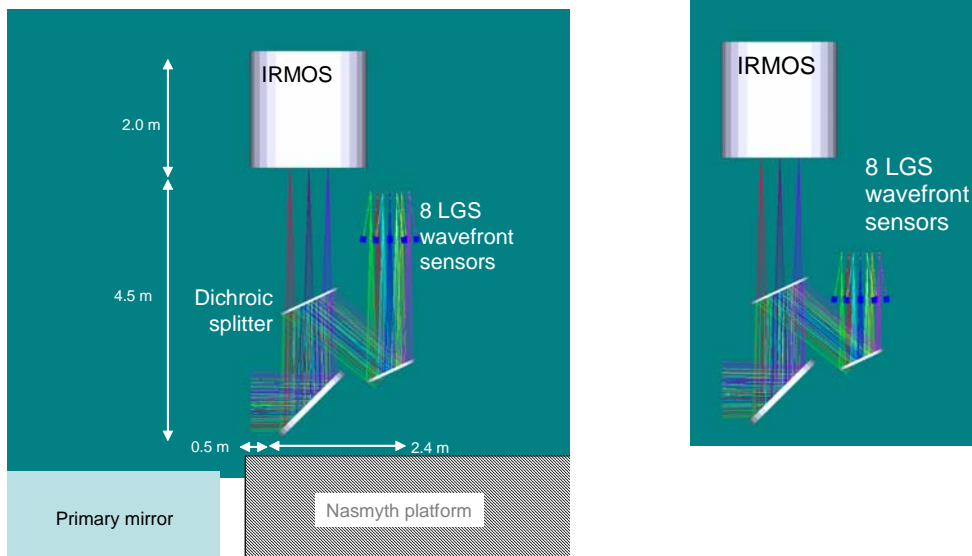


Figure 12. IRMOS with LGS wavefront sensors conjugate to 90 km (left) and 180 km (right).

Figure 13 shows a detail of the wavefront sensor design. Converging light from the telescope enters from right and is collimated by a small 25 mm diameter lens. The light reflects off the pupil mirrors (depicted as white circles at left; the diameter shown is 100mm) and then is relayed via a two-element telescope to a lenslet array. A second two-element relay then images the Shack-Hartmann dots onto the CCD, which is depicted as a 100mm blue cube. Each ray color in the figure represents light from a different LGS.

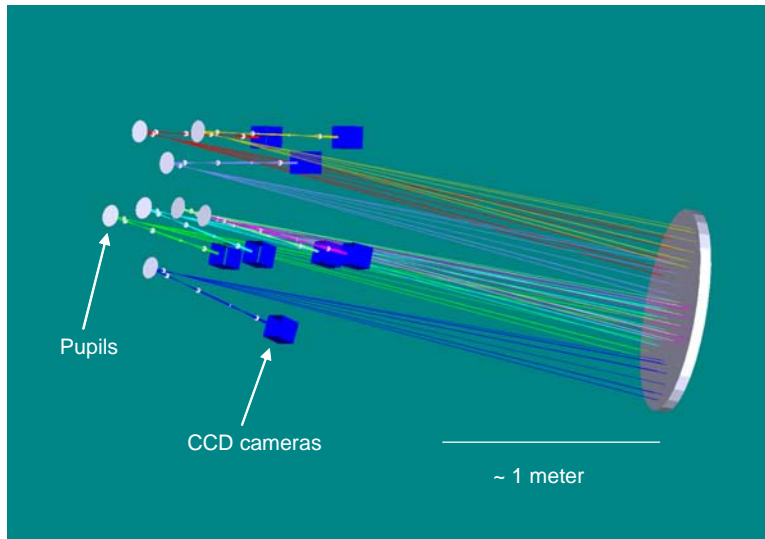


Figure 13. Details of the wavefront sensors.

The wavefront sensors will see roughly one wave peak to valley wavefront aberration from the telescope primary/secondary at the 2.5 arcminute off-axis location when imaging laser guidestars at zenith. The aberration will change with zenith angle. Since the

aberration is not too severe, it is conceivable that a lookup table with reference centroid offsets will suffice. The alternative is to put low-order DMs at the WFS pupil images whose figure can be slowly adjusted to overcome the telescope aberration.

9. MOAO Relay Design

9.1. Consequence of no pupil relay

First off, we should discuss the option of building the MOAO stage without a pupil relay. This would eliminate the need for a number of powered optics and thus reduce the emissivity, improve throughput, and simplify the design. However, this would not be a good choice optically, since if the DM were simply placed 600 mm behind focus (a place where the f/15 beam has expanded to roughly the size of the MEMS DM), then it would be at a conjugate altitude of +340 km. The Fresnel number for the 30 meter aperture is about $(50)^2$ there, meaning that features on the pupil of sizes smaller than about 1/50 of the pupil are completely blurred out by diffraction. This would defeat our objective of correcting the wavefront at scales of 1/100 of the aperture diameter.

9.2. Relay design

This discussion covers the design of MOAO units to be deployed in the image plane, as opposed to designs that have pick-off mirrors to kick the light out to units outside the image field (the CIT “TiPI” concept). Much of the same analysis probably could be used in the pick-off mirror configuration, though. This note covers the envelope of MOAO units rather than the performance, which will be covered in a subsequent note. The performance is generally, though, pretty good.

Assumptions:

- MOAO unit feeds some type of spectrograph
- Wavefront sensing is handled separately from the MOAO unit
- MOAO unit deployed in the image plane
- Real estate that MOAO consumes in focal plane should be minimized
- Either DM has sufficient stroke to correct the entire wavefront error or the secondary or MOAO relay mirror can act as a woofer.
- DM will be assumed to be coincident with the cold stop in order to minimize the number of surfaces
- The f# of the beam entering the spectrograph is probably not the same as that from the telescope—f/100 is assumed, based on e-mails with James Larkin (but this will turn out to be not that important of an assumption).
- For simplicity, the exit pupil of the telescope will be assumed to be at infinity, which is a pretty good assumption considering the focal lengths involved.

Many equations will be simplified by assuming relatively small fields: 2-5 arcsec diameter.

The simplest configuration (i.e., smallest envelope) is a 2 mirror configuration. An even number of mirrors is desirable so that the spectrograph or fibers are not in the way of the

image plane. The general form of the design is shown in Figure 14; a zoomed in version is in Figure 15. The relay optic would most likely be an off-axis ellipsoid with the cass image and the final image at the ellipsoid's foci.



Figure 14: Two mirror general design for MOAO. Light from the telescope enters at left; the spectrograph would be at right.

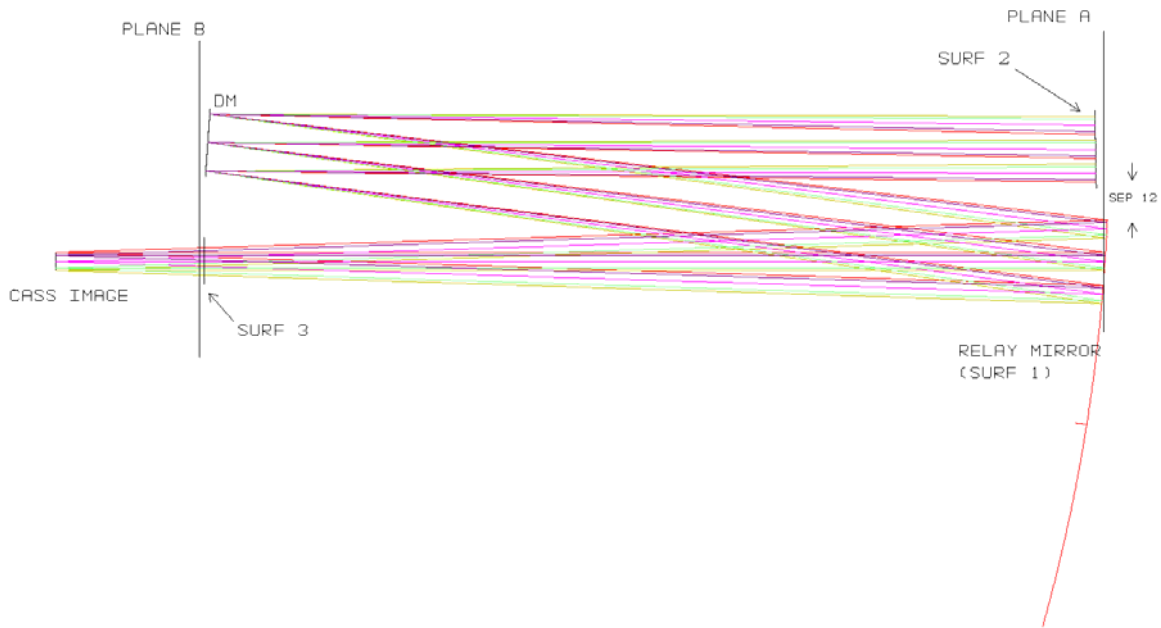


Figure 15: Zoomed-in view of general MOAO design.

The envelope at plane A must encompass the footprint on the relay optic as well as the beam passing by the relay optic (after reflection from the DM). Of course, there is also some separation, sep_{12} , between these footprints. If the footprint on the relay optic has diameter d_1 and the footprint of the by-passing beam has diameter d_2 , then it can be shown that the overall footprint in the long axis is

$$\begin{aligned}
 h &= d_1 + d_2 + sep_{12} = 2(DM \text{ size}) + 2(\text{field size}) + sep_{12} \\
 &= 2[(DM \text{ size}) + (\text{field size})] + sep_{12}
 \end{aligned}$$

sep_{12} can be small, perhaps a few mm. “Field size” is a linear, not angular, dimension, i.e., measured in mm. By scaling this equation by the plate scale, it can be expressed in terms of arcseconds.

Note that h is *independent of the output f -number*. A little thought shows why this is true. The radius of a footprint is equal to the sum of the chief ray height and the marginal ray height. The chief ray height at surfaces 1 and 2 must be the same because the DM is nominally flat, the chief ray height is zero at the DM, and surfaces 1 and 2 are the same distance from the DM. Now, because the beam is converging after the relay optic, the marginal ray heights at surface 1, the DM, and surface 2 are related by $y_1 > y_{DM} > y_2$. Again, because the DM is flat and the distances between the DM and surfaces 1 and 2 are the same, the difference between the marginal ray heights ($y_1 - y_{DM}$ and $y_{DM} - y_2$) must be the same. Therefore, the sum $y_1 + y_2 = 2y_{DM}$.

The width of the envelope at plane A (the short axis) is given by the larger of the footprint diameters, i.e, d_1 . It is straightforward to show that

$$\begin{aligned} d_1 &= 2(y_1 + \bar{y}_1) = 2y_{DM} \left(\frac{m+1}{m} \right) + 2\bar{y} \\ &= \left(\frac{m+1}{m} \right) (DM \text{ size}) + (field \text{ size}) \\ &\approx \frac{h}{2} \end{aligned}$$

“ m ” is the magnification of the relay ($f\#_{out}/f\#_{in}$) and is taken to be positive, so $\left(\frac{m+1}{m} \right)$ is close to 1 for m significantly larger than 1. Thus, for a separation significantly less than DM size and/or field size, the envelope width is approximately half of the envelope height (i.e., 2:1 aspect ratio).

Conclusion: The envelope at plane A has height $2[(DM \text{ size}) + (field \text{ size})] + sep_{12}$ and width $\left(\frac{m+1}{m} \right) (DM \text{ size}) + (field \text{ size})$. For small separations, this envelope has a 2:1 aspect ratio. If the field is small compared to the DM size, the short dimension is approximately equal to the size of the DM.

The envelope at plane B encompasses the DM and the by-passing input beam (surface 3) near the cass focus, as well as a separation between the two. The width of this envelope is just the DM size if the field is significantly smaller than the DM. The height of the envelope will actually be similar to the height at plane A. If one made the separation between the DM and surface 3 small, then the output beam would be slanted upward and put the image well above the input optical axis, thus creating a very tall envelope. Much more likely is to place the DM so that the output optical axis is nearly parallel to the input optical axis.

Not included yet is the presence of any mechanical components nearby, such as a cold stop or vacuum enclosure. If the MOAO unit is itself a vacuum enclosure, then we need to include the thickness of the vacuum vessel wall, which may be on the order of a

several mm; a better estimate would be helpful. If the MOAO unit is inside a larger vessel (say, containing several MOAO's and a large window on the front), then we may not need to include the thickness of the vacuum vessel.

The envelope at the image plane (excluding the spectrograph/fiber itself) is just the size of the field, which is $m(\text{field size})$. The final image plane will be located $(DM \text{ size})(\text{output } f\#)$ away from the DM. This is the length of the entire MOAO envelope.

Neglecting items such as a vacuum enclosure and beam clearance, an MOAO designs with a slow output $f\#$ will have an envelope with height approximately equal to $2(DM \text{ size}) + 2(\text{field size})$, and width approximately equal to the DM size.

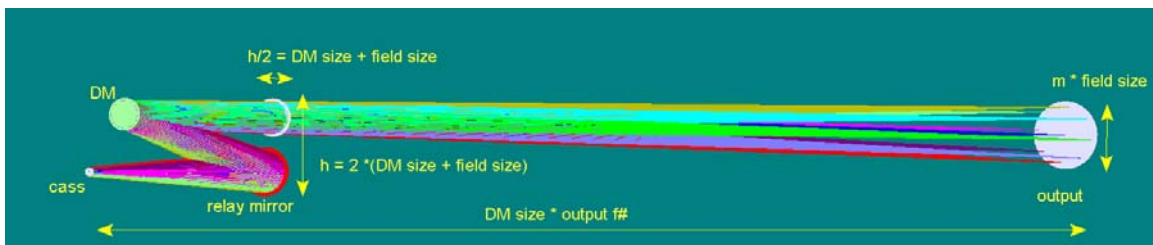


Figure 16. Perspective drawing of AO relay optics, showing envelope calculations.

Table 8 and Figure 17 below show the results of envelope calculations for a variety of DM sizes and telescope $f\#$'s (including a 5mm beam clearance consideration):

Table 8. Envelope calculations for IRMOS AO relay optics

DM size (mm)	Telescope $f\#$	Field size (arcsec)	Separation (mm)	Envelope height (mm)	Envelope width (mm)	Envelope length (mm)	Envelope height (arcsec)	Envelope width (arcsec)
10	16	2	5	29.3			12.6	
20	16	2	5	49.3			21.2	
30	16	2	5	69.3			29.7	
10	22	2	5	32.8			10.2	
20	22	2	5	52.8			16.5	
30	22	2	5	72.8			22.8	

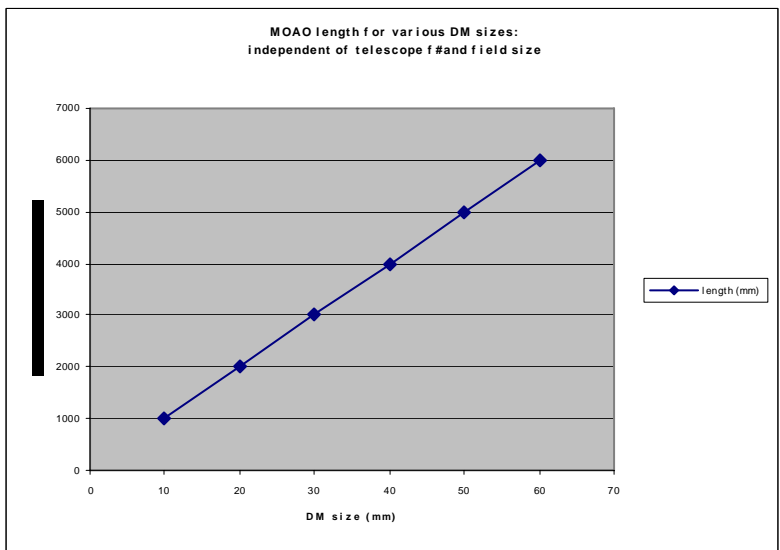
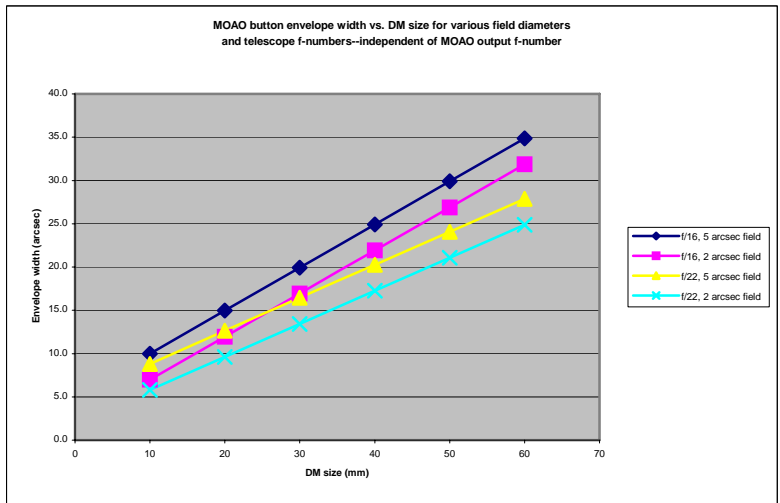
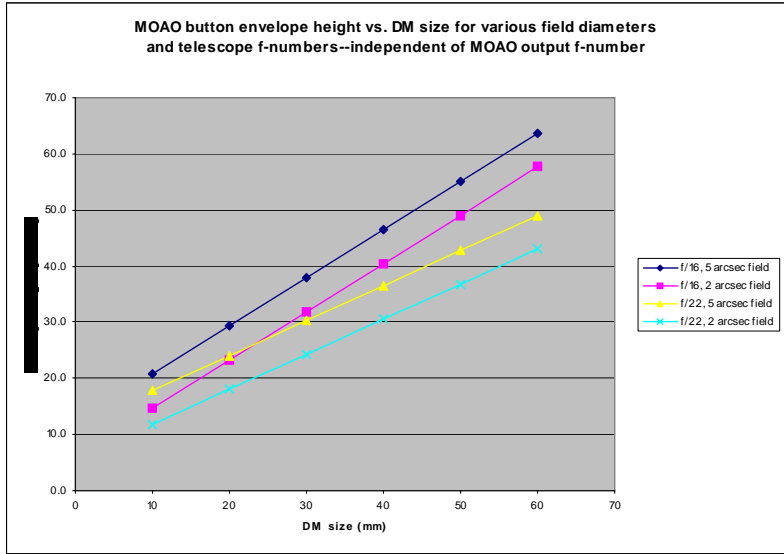


Figure 17: Envelope of MOAO buttons: height and width in arcseconds, length in mm.

10. IRMOS Staging Options

- 10,000 actuator MEMS DM (baseline): This option will meet the SRD requirements for IRMOS, with 50% ensquared energy at $\lambda = 1.1 \mu$. A MEMS DM of this size has yet to be built, but progress is being made such that by the time of deployment of IRMOS on TMT, it should be available.
- 4,000 actuator DM: This is now being developed for the Gemini Planet Imager under a consortium and is due to be delivered at the end of 2007. This will be slightly less capable at the shorter wavelength bands due to fitting error (112 nm vs 78 nm).
- 1,000 actuator DM: This device can be purchased now. It would meet the SRD requirements in the K band with 50% ensquared energy at 2.2μ . It has a stroke of 2μ surface so it would need a woofer DM, as would all the other viable MEMS DM options.
- No DM: This is the option to put a flat in place of DM in anticipation of a later upgrade. The woofer DM will provide some correction, but it will be very disappointing. Fitting error (about 700 nm with a 6x6 woofer and 350 nm with AM2) will dominate and SRD requirements will not be met in any band.
- IRMOS behind NFIRAOS: This would avoid the need to have an IRMOS AO system, but would pass only a 2 arcminute diameter field.
- IRMOS high Strehl superbutton: Having one MOAO unit that can produce a diffraction-limited image would allow a high resolution IFU spectrograph such as IRIS to be placed behind it. This AO button would differ from NFIRAOS in that wavefronts would be sensed and corrected open-loop as they are for other IRMOS AO units. It would require the addition of IR wavefront sensors and associated AO systems for correcting the tip/tilt stars in order to achieve diffraction-limited tip/tilt performance over a reasonable portion of the sky.

11. References

- ¹ Tokovinin and M. LeLouarn, *Isoplanatism in a multiconjugate adaptive optics system*, **J. Opt. Soc. Am. A**, Vol. 17, No. 10, Oct., 2000, pp. 1819-1827.
- ² Science-Based Requirements Document (SRD) v15.0 Instrument RFP Release, TMT.PSC.DRD.05.001.CCR15, Feb., 2006.
- ³ Andrei Tokovinin and Elise Viard, *Limiting precision of tomographic phase estimation*, **J. Opt. Soc. Am. A**, Vol. 18, No. 4, April, 2001, pp. 873-882.
- ⁴ Gavel, D., *Tomography for multiconjugate adaptive optics systems using laser guide stars*, **SPIE Astronomical Telescopes and Instrumentation**, Vol. 5490, June, 2004, pp. 1356-1373.
- ⁵ Clare, R., *Sky coverage results for IRMOS*, TMT.AOS.TEC.05.069.DRF01, Sept., 2005.
- ⁶ Herriot, G., *NFIRAOS Interim Review Status*, TMT.AOS.PRE.05.073.REL03, Nov., 2005.
- ⁷ Gavel, D., *MOAO PSFs and Ensquared Energies vs LGS Constellation*, TMT.AOS.TEC.05.030.DRF01, July., 2005.
- ⁸ Gavel, D., *MOAO Ensquared Energy for the 5+3 Guidestar Constellation*, TMT.AOS.TEC.05.046.DRF01, Aug., 2005.
- ⁹ Baker, K. L., Stappaerts, E. A., Gavel, D., Tucker, J., Silva, D. A., Wilks, S. C., Olivier, S. S., Olsen, J. A., *Adaptive compensation of atmospheric turbulence utilizing an interferometric wavefront sensor and a high-resolution MEMS-based spatial light modulator*, **Proceedings of the SPIE**, Volume 5553, Oct., 2004, pp. 269-280.
- ¹⁰ Evans, J.W., K. Morzinski, L. Reza, S. Severson, L. Poyneer, B. A. Macintosh, D. Dillon, G. Sommargren, D. Palmer, D. Gavel, and S. Olivier, *Extreme adaptive optics testbed: high contrast measurements with a MEMS deformable mirror*, **Proceedings of the SPIE**, Volume 5905, Sept., 2005, pp. 303-310.
- ¹¹ Evans, J. W., Morzinski, K., Severson, S., Poyneer, L., Macintosh, B., Dillon, D., Reza, L., Gavel, D., Palmer, D., Olivier, S., Bierden, P., *Extreme adaptive optics testbed: performance and characterization of a 1024-MEMS deformable mirror*, **Proceedings of the SPIE**, Volume 6113, Jan., 2006, pp. 131-136.
- ¹² Gavel, D., *MEMS Status and Potential Impact for AO Systems on TMT*, (view graph #8), TMT.AOS.PRE.06.005.REL01, Jan., 2006.
- ¹³ Noll, R.J., *Phase estimates from slope-type wave front sensors*, **J. Opt. Soc. Am.**, 68, 1978, pp 139-140.
- ¹⁴ Vogel, Curtis R.; Yang, Qiang, *Modeling and open-loop control of point-actuated, continuous facesheet deformable mirrors*, **Proceedings of the SPIE**, Volume 6272, July, 2006.